Optical manipulation of single magnetic beads in a microwell array on a digital microfluidic chip

Optical Manipulation of Single Magnetic Beads in a Microwell Array on a Digital Microfluidic Chip

*Deborah Decrop [a], Toon Brans [b], Pieter Gijsenbergh [c], Jiadi Lu [a], Dragana Spasic [a], Tadej Kokalj [a], Filip Beunis [b], Peter Goos [a,d], Robert Puers [c] and Jeroen Lammertyn [a]**

[a] Department of Biosystems, MEBIOS - Biosensors, KU Leuven, Willem de Croylaan 42, 3001 Leuven, Belgium

[b] Department of Electronics and Information Systems (ELIS) and Center for Nano and Biophotonics (NB-Photonics), UGent, Sint-Pietersnieuwstraat 41, 9000 Gent, Belgium

[c] Department of Electrotechnical engineering (ESAT-MICAS), KU Leuven, Kasteelpark Arenberg 10 postbus 2440, 3001 Leuven, Belgium

[d] Faculty of Applied Economics, University of Antwerp, Stadscampus Prinsstraat 13, 2000 Antwerp, Belgium

* Authors to whom correspondence should be addressed:

Mailing address: BIOSYSTEMS-MEBIOS Biosensors, KU Leuven, Willem de Croylaan 42, 3001 Leuven, Belgium

Phone: +3216321459

Fax: +3216322955

E-mail: Jeroen.lammertyn@kuleuven.be

Abstract

The detection of single molecules in magnetic microbead microwell array formats revolutionized the development of digital bio-assays. However, retrieval of individual magnetic beads from these arrays has not been realized until now despite having great potential for studying captured targets at the individual level. In this paper, optical tweezers were implemented on a digital microfluidic platform for accurate manipulation of single magnetic beads seeded in a microwell array. Successful optical trapping of magnetic beads was found to be dependent on Brownian motion of the beads, suggesting a 99% chance of trapping a vibrating bead. A tailor-made experimental design was used to screen the effect of bead type, ionic buffer strength, surfactant type and concentration on the Brownian activity of beads in microwells. Using the optimal conditions the manipulation of magnetic beads was demonstrated by their trapping, retrieving, transporting and repositioning to a desired microwell on the array. The presented platform combines the strengths of digital microfluidics, digital bio-assays and optical tweezers, resulting in a powerful dynamic microwell array system for single molecule and single cell studies.

Introduction

Microfluidic microarray systems have emerged over the years as powerful tools for divers biomedical applications, including genomics[1], proteomics[2–4], drug screening[5–7], disease diagnosis[8] and multiplexed screening for biomolecular interactions[9]. Based on the arraying method, microarrays are usually classified into static and dynamic. In static arrays biomolecules are immobilized as microspots on a solid support, by e.g. microcontact printing[4], whereas in dynamic arrays biomolecules are typically coupled to microcarriers, such as beads[10–13] or microrafts[14] that are subsequently seeded in the array. Using beads as microcarriers offers several advantages like (i) straightforward surface functionalization due to many established immobilization strategies for a broad range of bioreceptor molecules (e.g. DNA, RNA, antibodies), (ii) higher binding efficiency due to the high surface-to-volume ratio of microcarriers, resulting in an improved limit of detection and reaction kinetics[10,12,15], and (iii) facilitated reagent delivery and signal generation, achieved by active mixing of beads and their seeding in arrays, typically using continuous flow or digital microfluidic (DMF) systems[11–14,16].

It has been previously demonstrated that seeding of beads in arrays can be realized by their trapping with valves[12] or micro-sized structures[17], patterning surfaces with a monolayer of beads[18] or by sealing beads in femtoliter-sized microwells. The latter is often used for the development of digital bio-assays[19,20] where individual target molecules are captured on beads, seeded in the microwells and detected at the single target level reaching ultimate sensitivities[2,4,20]. Sealing of beads in femtoliter reaction chambers ensures generation of highly confined enzymatically generated fluorescent signals in those microwells containing a bead that captured a target molecule. The use of magnetic beads is preferred in this approach since the seeding efficiency can reach up to 99% when assisted by the application of a magnetic force[19], compared to only 40% to 60% when no magnetic forces are applied[20].

Although microbead array technology is mainly used for target detection, its unexplored potential lies in the retrieval of single magnetic beads from the microwell array[13,21] and post-analysis of captured targets, such as DNA (e.g. polymerase chain reaction (PCR) or sequencing), bacteria (e.g. culturing), cells or microvesicles (e.g. lysis and cargo analysis). Over the past years, several groups have developed tools to selectively manipulate beads or cells in trap-and-release systems using active methods (e.g. electric, magnetic, acoustic or optical forces)[13,21–24] or passive methods (e.g. dynamic changes in the flow field)[12,13,25]. However, despite its great potential, the combination of microwell-arrays based microfluidics and optical tweezers has been mainly limited to the isolation, transportation or deposition of cellular targets[26–33]. Enabling the manipulation of single magnetic beads on a digital microfluidic platform would include a broader range of targets (e.g. DNA, viruses, proteins), making microbead array technology more versatile as life science research tools and for diagnostics (e.g. single exosome isolation and subsequent analysis of the molecular cargo[34,35]). The advancement is, however, hampered by the fact that magnetic beads are more tricky to trap with optical tweezers because of (i) the energy-absorbing iron particles in the polystyrene matrix[36–38], and (ii) the attraction forces between sedimented magnetic beads and the microwell surfaces[39].

This paper reports on the integration of an in-house built optical tweezers set-up with a digital microfluidic platform for accurate manipulation of single magnetic beads trapped in a microwell array. The importance of Brownian motion of beads for their optical manipulation is investigated as well as the fraction of magnetic beads showing Brownian motion in function of several parameters, including the bead type, ionic buffer strength, surfactant type and concentration. This study focuses on

carboxylated and streptavidin coated beads since these two types of beads are commonly used in digital bio-assays. Six different non-ionic surfactants that are generally used in combination with biomolecules and cells are tested. The selected conditions are experimentally confirmed and implemented to demonstrate various single bead manipulation concepts on the DMF-platform.

Experimental section

Materials

Carboxylated and streptavidin coated LodeStar magnetic beads (2.7 µm diameter) were purchased from Agilent Technologies (Santa Clara, CA, USA). Fluorinert FC-40 was obtained from 3M (St. Paul, MN, USA). All photolithography reagents were obtained from Rohm and Haas (Marlborough, MN, USA) while Parylene-C dimer and Silane A174 were purchased from Plasma Parylene Coating Services (Rosenheim, Germany). Teflon-AF® (6% w/w in FC-40) was obtained from DuPont (Wilmington, DE, USA). CR-7 chromium etchant was obtained from Cyantek (Fremont, CA, USA). The fluoroalkylsilane DynasylanF8263 was a generous gift from Evonik Degussa International AG (Essen, Germany). Borosilicate cover slides were obtained from VWR international and Tween 40, Tween 60, Tween 80, Pluronic-F68 and 4',6-diamidino-2-phenylindole (DAPI) were purchased from Sigma-Aldrich (Saint Louis, MO, USA). Tween 20 and Brij 35 were obtained from Fisher scientific (Waltham, MA, USA). Oligonucleotides with a biotin group at the 5'-position and a fluorescein (FAM) or Cyanine3 (Cy3) group at the 3'-position were synthesized by IDT (Integrated DNA technology, Leuven, Belgium).

DMF-chip fabrication and magnetic bead seeding

For the optical manipulation of single magnetic beads, double plated DMF-devices with microwell arrays were fabricated as described earlier[19,40] and in Supporting Information. As shown in **Figure 1A**, the electrode-plate contains a pattern of chromium actuation electrodes whereas the microwell-plate has a grounding electrode with a transparent window including the microwell array. This microwell array, fabricated in the Teflon-AF® layer, contains 62500 microwells, with dimensions (4 µm width, 3 µm depth) specifically chosen to accommodate one magnetic bead of 2.7 µm diameter. Larger or smaller microwell dimensions will have an adverse effect on either single bead seeding

or the subsequent printing of femtoliter droplets. For seeding, magnetic beads were first suspended in a buffer solution under investigation. A 2.5 µL droplet, containing approximately 200000 beads, was used for seeding the microwell array. Using the electrowetting-on-dielectric (EWOD) concept, the droplet was shuttled back and forth over the microwell array while keeping a magnet on top to attract magnetic beads in the microwells, as illustrated in **Figure 1B.**

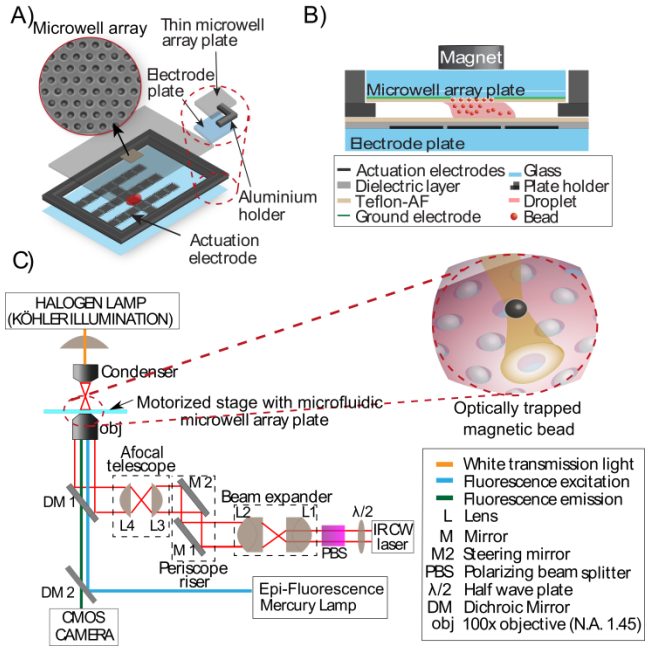

Figure 1: Schematic illustration of A) the assembly of the digital microfluidic electrode- and microwell array-plate with a zoom-in of the microwell array; B) the mechanism of magnetic bead seeding; C) the assembly of the optical components into the optical tweezers platform with a zoom on the optical trapping of a magnetic bead.

Optical tweezers set-up

For the optical trapping of individual magnetic beads, an optical tweezers set-up was home built with optical components mounted on a vibration isolated optical table, as illustrated in **Figure 1C** and described in more detail in Supporting Information. The construction was based on the design of Lee et al[41]. A Nikon *Ti-Eclipse* inverted microscope (Nikon, Japan) equipped with a CFI Plan Apochromatic 1.45-NA 100x oil-immersion objective and a Cobolt Rumba TM (1064 nm), 500 mW DPSS-SLM continuous wave laser system (Laser 2000 Benelux CV) were used to build the optical path.

Brownian motion of magnetic beads for selective trapping

Brownian motion and optical trapping of magnetic beads seeded in the microwell array was tested in a buffer solution commonly used on the DMF-platform for droplet movement. Carboxylated and streptavidin coated beads were suspended in 1× PBS with 0.1% Tween 20. A 2.5 µL droplet was used for seeding. After seeding, the magnet was removed with gravity being the sole force pressing the beads against the surface. Seeded microwell arrays were immediately observed under a bright field microscope at 100× magnification. The region of interest (ROI) was restricted to ~ 100 beads and used for taking a 5 min movie at 15 frames-per-second for observing the presence of Brownian motion (ON/OFF). Since the Brownian movement could be easily observed by eye, the number of beads with Brownian motion was determined manually in each movie. Subsequently, the same 100 beads were tested for trapping with the optical tweezers. This procedure was repeated six times, at random positions on the microwell array, resulting in a total of ~ 600 beads for which the presence of Brownian motion and successful optical trapping was studied.

Experimental design and data analysis for Brownian motion of magnetic beads

Several factors, like bead type, buffer pH, ionic buffer strength, surfactant type and concentration (listed in **Table 1**) were tested for their influence on the Brownian motion of seeded magnetic beads through optimally designed experiments. An initial D-optimal experimental screening design[42] (see Supporting Information) was used to study the impact of these five factors on the interaction of beads with glass and Teflon-AF® surfaces. For all tested conditions, beads were seeded in a microwell array and immediately observed under a bright field microscope at 60× magnification. The ROI was restricted to ~ 260 beads and used for taking a 5 min movie at 15 frames-per-second for further analyzing the presence of Brownian motion (ON/OFF). This procedure was repeated six times, at random positions on the microwell array, resulting in a total of ~ 1600 analyzed beads per condition. The obtained fractions of beads with Brownian motion were used as the dependent variable of a logistic regression analysis with the five experimental factors as independent variables.

Subsequently, a new I-optimal follow-up experimental design was implemented for both carboxylated and streptavidin coated beads to test the desirability of higher surfactant concentrations for two surfactant types, at fixed ionic buffer strengths (factors listed in **Table 1**). The fractions of beads with Brownian motion were obtained as described before and used as the dependent variable of a regression analysis using a least squares fit. Construction of

experimental designs, statistical analysis and data interpretation were performed using the JMP Pro 11 statistical package (SAS Institute Inc., Cary, NC)[42,43].

Table 1: Overview of different factors and their levels used for the initial and follow-up experimental design for both carboxylated and streptavidin coated beads.

	Initial Design	Follow-up Design	
Factor	**Levels**	**Levels**	**Levels**
Bead type	Carboxyl (COOH) / Streptavidin (STREP)	Carboxyl (COOH)	Streptavidin (STREP)
Surfactant type	Brij 35 / Pluronic-F68 / Tween 20 / Tween 40 / Tween 60 / Tween 80	Tween 40 / Tween 60	Tween 40 / Tween 60
Ionic Buffer strength	0.1× PBS / 1× PBS / 10× PBS	7× PBS	1× PBS
pH	6.4 / 7.4 / 8		
Surfactant concentration (v/v%)	0.05 / 0.1 / 0.5 / 1	1 / 1.5/ 2	1 / 1.5 / 2

Bead functionalization and characterization

To demonstrate the bead manipulation on the DMF-chips, magnetic beads were functionalized with three fluorophores. Carboxylated magnetic beads (2.7 µm) were functionalized with DAPI using EDC-chemistry in a one-step protocol. Hereto, beads (2.3×10^5 beads/µL) were washed four times with MES buffer (25 mM, pH 5) and incubated with a fresh EDC/NHS-solution (each 50 µg/µL) for 30 min at room temperature on a tilt–and-rotation device. Next, beads were incubated with DAPI solution (0.6 µg/µL) for 1 h and subsequently any remaining non-reacted activated carboxylgroups were quenched with 50 mM Tris buffer (pH 7.4) for 30 min at room temperature on a tilt-and-rotation device. Streptavidin coated magnetic beads (2.7 µm) were functionalized with FAM- or Cy3-linked oligonucleotides using streptavidin-biotin binding (see **Table S1** of Supporting information for sequences). Beads (2×10^5 beads/µL) were washed three times with 10 mM Tris-HCl (300 mM NaCl, 1 mM EDTA, pH 7.5) followed by incubation with 1 µM biotinylated-DNA (FAM or Cy3 labelled) for 45 min at room temperature on a tilt-and-rotation device. Unbound DNA was removed and the beads were washed three times with PBS. All beads were stored in 1× PBS until they were used. Fluorescently labelled beads were visualized using fluorescence microscopy with three different filter channels (DAPI, FITC and TRITC). Multicolour images were obtained by stacking the three acquired fluorescent images, allowing discrimination of colours.

A Malvern Zetasizer Nano system was used for zeta potential measurements of the carboxylated, streptavidin coated and fluorescently functionalized beads. NIR spectroscopy (Perkin Elmer, Lambda 950) was performed to study which beads were most

prone to thermal heating. A detailed description of these experiments can be found in Supporting information.

Results and discussion

Studying the importance of magnetic bead Brownian motion for selective trapping

When trapping optically dense magnetic beads, laser energy gets absorbed by both the bead and its surrounding medium leading to possible thermal damage of tethered biological samples[44]. To avoid damaging of biological samples optically less dense magnetic beads should be used. NIR absorbance measurements were performed on magnetic LodeStar and Dynabeads®, as well as on non-magnetic polystyrene and silica beads. These indicated 27% less absorption of magnetic LodeStar beads at 1064 nm, the wavelength of the optical tweezers, compared to magnetic Dynabeads® (**Figure S3**). Despite their low absorption, polystyrene or silica beads were not preferred since they lack magnetic properties required for seeding the microwell array with high efficiencies. Linking this information to earlier reported results that have proven that laser irradiation (1W for 40 sec) of magnetic Dynabeads® does not have a negative effect on PCR reagents[45], it was decided to use LodeStar beads for the optical trapping experiments.

The random motion of microbeads in a solution, known as Brownian motion, is attributed to collisions of molecules of the medium with the microbeads and is proven to be temperature dependent[46–48]. As a first step, the importance of Brownian motion of magnetic beads, confined in a microwell, was examined for optical bead trapping. Magnetic beads were seeded in a microwell array and immediately observed under the bright field microscope at 100× magnification. The ROI was restricted to ~ 100 beads and the number of beads exhibiting Brownian motion was determined. Subsequently, the same ~ 100 beads were tested for optical trapping. This was repeated at 6 random positions of the microwell array resulting in a total of ~ 600 beads analysed per sample. For this test, both negatively charged carboxylated beads and nearly uncharged streptavidin coated beads were used. A 1× PBS with 0.1% Tween 20 buffer, which is commonly used on the DMF-platform for droplet movement, was used for this experiment. As can be seen in **Figure 2**, 35% of the carboxylated beads and 27% of the streptavidin coated beads displayed Brownian motion within the microwells. After testing optical trapping of both Brownian and non-Brownian

magnetic beads, two observations could be made: (i) for both bead types, beads showing no Brownian behaviour could not get trapped into the focused laser beam, and (ii) among beads with Brownian motion, optical trapping was successful for 34% and 24% of the carboxylated and streptavidin coated beads, respectively, corresponding to trapping efficiencies of 95% and 91%.

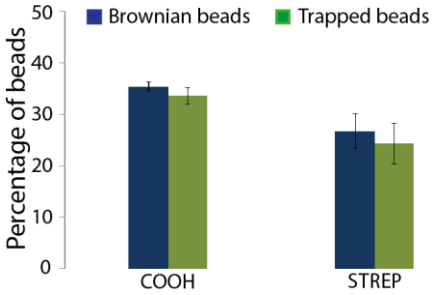

Figure 2: Bar graph showing the percentage of beads with Brownian motion and percentage of beads being optically trapped for carboxylated (COOH) and streptavidin (STREP) coated beads. Both bead types were suspended in 1× PBS with 0.1% Tween 20. Error bars indicate one standard deviation obtained from three independent repetitions, each with ~ 600 beads.

Based on these results it was concluded that optical manipulation of magnetic beads was only successful for those beads displaying Brownian motion. However, merely a small percentage of seeded magnetic beads displayed this Brownian behaviour. A large fraction of seeded magnetic beads adhered to the microwell surfaces due to a combination of surface interactions (electrostatic, Van der Waals, steric, hydrophobic and hydration forces) and therefore showed no Brownian motion. The next step was to increase this fraction of beads with Brownian motion by optimizing factors influencing the surface interactions, like bead functionalization, ionic buffer strength, buffer pH, surfactant type and concentration.

Optimal design of experiments for increasing Brownian motion of superparamagnetic beads

As observed in the previous section, a small percentage of magnetic beads showed Brownian motion in their microwell using a 1× PBS buffer with 0.1% Tween 20 for seeding of beads in the microwell array. In order to increase this percentage several factors were tested, including surfactant type and concentration, buffer pH, ionic buffer strength and bead type (**Table 1**). Because of the large number of factors, an initial D-optimal experimental screening design[42] was set up, making experimental

testing practically more feasible. The fraction of beads showing Brownian motion was determined for each experimental condition (as described in Experimental section) and the experimental outcomes were processed in three steps: (i) construction and validation of a regression model, (ii) identification of significant factors and (iii) determination of optimal buffer conditions (i.e. including all factors). More details on the experimental design and statistical analysis are provided in Supporting Information (Optimal design of experiments).

The obtained fractions of beads with Brownian motion were first logistically transformed and then used as the dependent variable of the model. A regression model was estimated using least squares estimation, and the goodness of fit was assessed using diagnostic tests. Using this regression model and its corresponding mathematical expression (see **Eq. 2** of Supporting information), predicted fractions of beads with Brownian motion, also called predicted response, were calculated. The analysis of variance (ANOVA) showed that the regression model had a strongly significant explanatory value ($p < 0.0001$) and as a result the predicted (Yc) and observed fraction of beads with Brownian motion were highly correlated (adjusted R^2 of 0.77) (**Figure S5**).

Using effects tests, the significant effects of the experimental factors were identified, allowing removal of non-significant factors (e.g., pH) from the model. The estimated coefficients of the final regression model and the effect tests of all significant factors (e.g., bead type, ionic buffer strength, surfactant type and concentration) are respectively listed in **Tables S6** and **S7**. The optimal settings as calculated with the statistical model differed for the two bead types due to a significant interaction effect between ionic buffer strength and bead type. For carboxylated beads, increasing the ionic buffer strength resulted in a larger predicted fraction of beads showing Brownian motion, with a response plateau at ionic buffer strengths ≥ 4× PBS (**Figure 3 A-C**). In contrast, for streptavidin coated beads, the predicted fraction of beads with Brownian motion reaches an optimum at about 1× PBS (**Figure 3 B-D**). Also, the effect of surfactant concentration was strongly positive for Tween 40 and Tween 60, while only weakly positive for the other surfactants, being overall slightly more positive in case of the carboxylated beads.

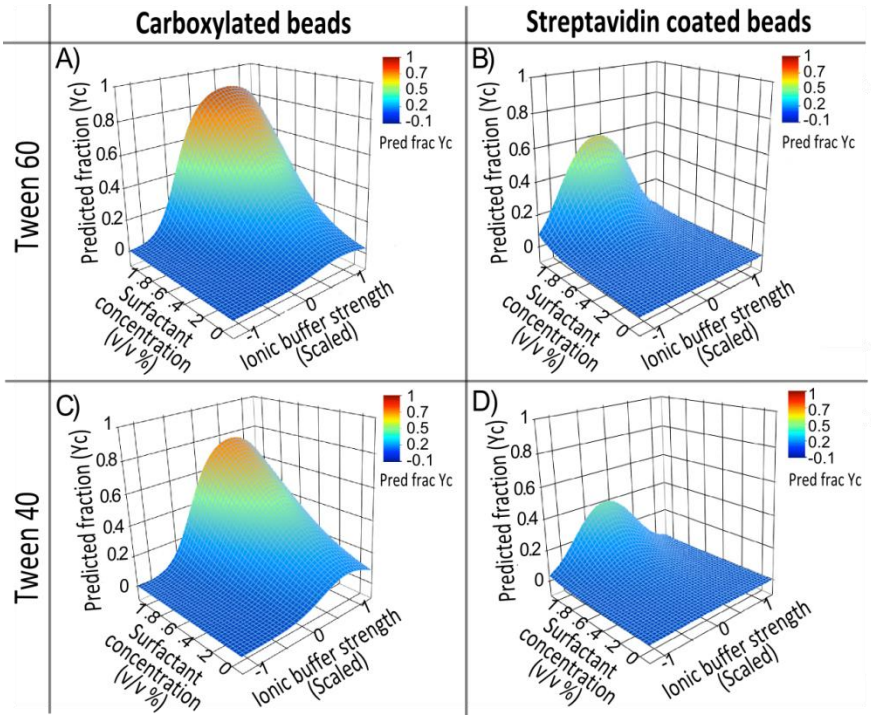

Figure 3: Surface plots of the predicted fraction (Yc) as a function of the Tween 60 concentration and ionic buffer strength for (A) carboxylated beads and (B) streptavidin coated beads. Surface plot of the predicted fraction (Yc) as a function of the Tween 40 concentration and ionic buffer strength for (C) carboxylated beads and (D) streptavidin coated beads. For all graphs the ionic buffer strength ranged from 0.1 to 10× PBS and was scaled to a range of [-1,1].

The constructed model including only the significant factors predicted a maximum fraction of beads with Brownian motion at 7× PBS with 1% Tween 60 for carboxylated beads and at 1× PBS with 1% Tween 60 for streptavidin coated beads (**Figure 3 A-B**). Likewise, for both bead types, adding 1% Tween 40 to the buffer also resulted in an increased fraction of beads with Brownian motion (**Figure 3 C-D**). The contour plots of the predictions for different buffer conditions as a function of all six surfactant types are shown in **Figure S8**.

The outcome of this initial screening experiment indicated that surfactant concentrations ≥ 1% were desired for both Tween 40 and Tween 60. Therefore, a follow-up I-optimal experimental design was implemented for both types of beads. I-optimal designs focus on precise predictions and emphasis on the center of the factor range allowing response predictions anywhere inside this range[42]. For this design, the concentrations of Tween 40 and Tween 60 were varied, keeping the ionic buffer strength constant (i.e. 7× PBS for carboxylated beads; 1× PBS for streptavidin coated beads) (see **Table 1**). The experimental results were processed separately for

carboxylated and streptavidin coated beads using the same three steps as before. A least squares fit of the data of the follow-up experiment led to large adjusted R^2 values (carboxylated beads: adjusted R^2 = 0.85; streptavidin coated beads: adjusted R^2 = 0.95). The newly estimated models (see **Eq. 3, 4, 5** and **6** of Supporting information) indicating the optimal surfactant concentrations for both bead types are shown in **Figure 4**. For carboxylated beads, the optimal concentrations of Tween 40 and Tween 60 were 1.5% and 1.3%, resulting in predicted percentage of beads with Brownian motion of 76% and 71%, respectively. For streptavidin coated beads, the optimal concentration of Tween 40 and Tween 60 were 2% and 1.5%, respectively, with prediction values of 50% and 79%, of the beads showing Brownian motion.

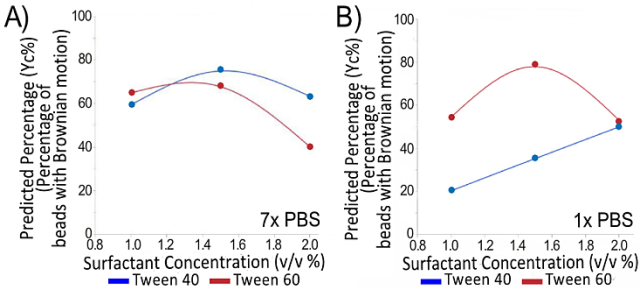

Figure 4: Regression plot of the predicted percentage (Yc%) as a function of surfactant concentration for A) carboxylated beads and B) streptavidin coated beads for Tween 40 and Tween 60 at a constant ionic buffer strength.

Interestingly, the analysis of the experimental designs indicated two major effects on the fraction of magnetic beads with Brownian motion: (i) a significant interaction effect of bead type and ionic buffer strength and (ii) a significant positive effect of surfactant type and concentration in case of Tween 40 and Tween 60. The increased fraction of beads with Brownian motion, as a function of these significant factors can be explained by surface interaction forces between magnetic beads and the microwell surfaces. The latter consist of hydrophobic Teflon-AF® side walls and a hydrophilic glass bottom. Magnetic beads are composed of iron nanoparticles embedded in a hydrophobic polystyrene matrix. In this bead-Teflon-glass configuration multiple surface interactions play a role. (i) attractive hydrophobic forces are present between the polystyrene matrix of the magnetic bead and the Teflon sides, while a repulsive force is present between the bead and glass bottom[49–56]. For carboxylated beads, carboxyl groups shield the hydrophobic polystyrene matrix reducing both the attractive force towards the Teflon sides and the repulsive force with the glass bottom[57]. Therefore, in general the percentage of magnetic beads showing

Brownian motion is higher for carboxylated beads compared to streptavidin coated beads. Streptavidin has hydrophilic and hydrophobic groups that shield this hydrophobic force less effectively. (ii) Functionalized magnetic beads also interact with the microwell surfaces according to electrostatic forces[58,59]. Electrostatic interactions result from the electrical potential (zeta potential) of the surfaces which is determined by factors like ionic buffer strength and surface functionality. Carboxylated and streptavidin coated beads have measured zeta potentials of respectively -73.5 ± 0.54 mV and -45.9 ± 1.79 mV, which increase with increasing ionic buffer strength (see **Figure S2**). Therefore, higher ionic buffer strengths were required for carboxylated beads which have a more negative zeta potential compared to streptavidin coated beads. This effect was indicated by the interaction effect predicted by our model. (iii) Non-ionic surfactants consist of polymer-like molecules that can adsorb onto the magnetic bead surfaces forming biolayers that cause steric interactions[60,61]. As indicated by the models this steric effect was strongly positive for both Tween 40 and Tween 60 and increased with the surfactant concentration.

Use of optimal buffer for selective magnetic bead trapping

The predicted optimal buffer conditions were next validated experimentally. This was done by using carboxylated beads as well as streptavidin coated beads functionalized with Cy3- and FAM-labelled DNA. Because DNA molecules are negatively charged at pH 7.4 of PBS buffer, functionalisation with DNA renders the beads more negative. Streptavidin coated beads, functionalized with Cy3- and FAM-labelled DNA, have respectively measured zeta potentials of -72.7 ± 0.8 mV and -71.2 ± 2.9 mV which corresponds to the measured zeta potential of carboxylated beads (-73.5 ± 0.5 mV) (see **Figure S2**). Therefore, the optimal buffers for carboxylated beads (7× PBS with 1.5% Tween 40 or 7× PBS with 1.3% Tween 60) were used in this experiment for both types of beads. **Figure 5A** shows that, when using 7× PBS with either 1.5% Tween 40 or 1.3% Tween 60, a high percentage of carboxylated and fluorescently labelled streptavidin coated beads showed Brownian motion and were subsequently trapped. When compared to the results of our first test, using 1× PBS with 0.1% Tween 20 (shown in Figure 2), more than double the percentage of beads displayed Brownian motion and were trapped when using optimal buffer conditions. **Figure 5B** shows the correlation (based on data from Figure 2 and 4B) between the percentage of beads with Brownian motion and percentage of trapped beads. With an adjusted R^2 of 0.99 it

can be concluded that there is a high correlation between beads with Brownian motion and bead trapping, indicating a 99% chance of trapping a vibrating bead. This correlation does not necessarily imply a causal relationship and further research is needed to clarify this.

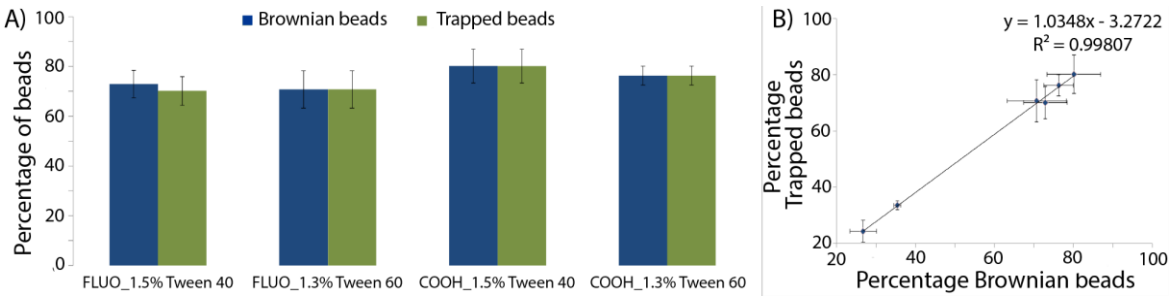

Figure 5: A) Bar graph showing the percentage of beads with Brownian motion and trapped beads for carboxylated (COOH) and fluorescently labelled (FLUO) streptavidin beads performed in 7× PBS with either 1.3% Tween 60 or 1.5% Tween 40. B) Correlation between trapped beads and beads showing Brownian motion with an R^2 of 0.99. All error bars represent one standard deviation obtained from three independent repetitions.

Magnetic bead retrieval, trapping, transportation and positioning

The interaction of a focused laser beam with a microbead results in a force of the beam on the bead[26,32,62]. Conventionally, this force is split up into two components. The gradient force results from refraction of the laser light and is directed towards the laser focus. A scattering force results from radiation pressure and pushes the bead along the beam axis. Depending on the balance between these two components, a bead is either pushed out of the microwell or trapped in the laser beam. **Figure 6** illustrates two mechanisms of magnetic bead manipulations that can only be done with those beads showing Brownian motion, using optical tweezers.

Depending on the relative position of the bead and the laser focus, two manipulation mechanisms were discriminated: bead release from the microwell array and bead trapping followed by transportation and repositioning. In the first scenario (**Figure 6A**) when a bead was approximately 5 µm above the laser focus, it experienced a high scattering force (> gradient force) and was pushed out of the microwell (bead retrieval). A vibrating bead, in this case, was retrieved from its microwell, into the droplet on top of the microwell array. Using this optical manipulation principle, identical beads were retrieved from a microwell array and pushed into the droplet above. Subsequently, the droplet was transported to a new

microwell array where the beads were reseeded. In a second scenario the bead was positioned between the objective and laser focus and it was pushed towards the equilibrium point, where it was stably trapped. This situation is shown in **Figure 6B** for trapping beads from a microwell, subsequently transporting it over the array surface and repositioning it in another microwell. Once the bead was positioned in the new microwell, the laser beam was shut-off and the optical trap released the bead, enabling it to settle in the new microwell. In the first scenario, the bead interacted only 2 to 4 seconds with the laser beam, whereas in scenario two the interaction time ranges between 10 to 60 seconds depending on the transportation distance. This maximal time of interaction was suggested acceptable according to what was reported earlier[45].

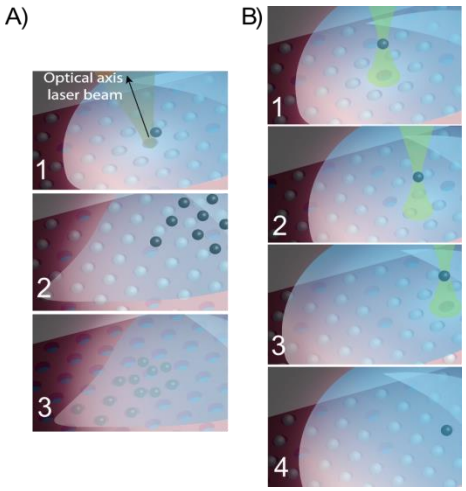

Figure 6: Two scenarios of magnetic bead manipulation with optical tweezers. The orientation of the laser beam is upward and is indicated with an arrow in the first image of A. A) The beads are pushed out of their microwells into the droplet positioned on top of the array (1). By transporting the droplet from one array to another (2), the beads can be reseeded in another microwell array (3). B) When a bead is stably trapped near the laser focus (1), it can be transported over the surface (2) and repositioned in a new microwell (3). Closing the laser beam allows for bead settling in the microwell (4).

For demonstration purposes (**Figure 7**), magnetic beads were functionalized with fluorophores of a different colour. Carboxylated beads were coated with DAPI (blue) using EDC/NHS chemistry, whereas streptavidin coated beads were functionalized with FAM (green) or Cy3 (red) terminated oligonucleotide strands using streptavidin-biotin binding. Multicolour images were obtained by stacking three fluorescent images, acquired using different filter channels, allowing discrimination of the different colours (**Figure 7A)**. In a first application, differently coloured beads were mixed and dissolved in 7× PBS with 1.5% Tween 40 to obtain a high number of

beads with Brownian motion. Next, magnetic beads were seeded in a microwell array, and subsequently only the e.g. red beads were selectively retrieved. **Figure 7B** shows the fluorescent images taken before and after retrieval of red beads from a section of the microwell array. Retrieved beads were floating freely in the droplet positioned on top of the array and this droplet was then transported, using the EWOD principle, to a new microwell array in which the red beads were reseeded. The fluorescent image taken from this new array (Figure 7B) demonstrated that only red beads were reseeded proving the specificity of the technique. Not only could beads be successfully retrieved from their microwell, they could also be trapped with the laser beam and transported over the microwell array to be repositioned at another location in the microwell array. Using this bead transportation and repositioning mechanism, structures such as "KUL" or a smiley were made (**Figure 7C**). The Supporting movie illustrates the assembly of a smiley.

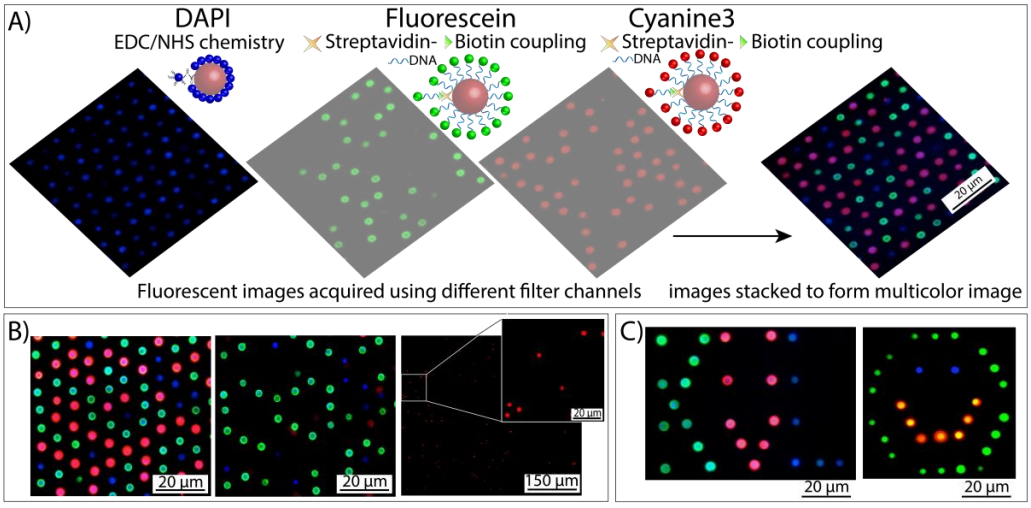

Figure 7: Fluorescence microscopy image of coloured beads. A) Carboxylated (blue) and streptavidin (green and red) beads functionalized with fluorophores. Mixtures of coloured beads are seeded in a microwell array and the images show a small frame of the array. Fluorescent images are taken using different colour filters, which are subsequently stacked to obtain a multicolour image. B) Left – mixture of coloured beads seeded in the array; Middle – only red beads are retrieved from their microwell; Right –red beads are reseeded in a new microwell array. C) Assembly of KUL and smiley by specifically positioning beads in the microwell array using optical tweezers.

Conclusion

In this work an optical tool for the manipulation of single magnetic beads, seeded in a microwell array, was developed by combining a single beam optical tweezers set-up

with a digital microfluidic chip containing a microwell array. Experimental results have shown that Brownian motion of beads, seeded in the microwells, is necessary to optically trap and hence manipulate the beads. Tailor-made designed experiments were used to build a predictive model for identifying optimal buffer conditions in which large fractions of beads showed Brownian motion within the microwell. The optimal buffer conditions proved to be suitable for beads functionalized with DNA and fluorophores. Using the final optimized buffer conditions, bead manipulations such as retrieval, trapping, transportation and repositioning were attained, suggesting that the developed platform is a powerful tool within the fields of genomics (e.g. post-analysis of DNA by PCR or sequencing), proteomics, disease diagnostics or single-cell analysis (e.g. culturing bacteria resistant to antibiotics treatment).

Acknowledgements

The research leading to these results has received funding from the Research Foundation - Flanders (FWO G086114N and G080016N), De Vlaamse Liga tegen Kanker (EXM C8744-A), the Hercules initiative for large equipment ("HELICOM", ZW11-15), the KU Leuven (OT 13/058 and IDO 10/012, IOF KP/12/009) and EU project Norosensor (FP7-NMP-2013-SMALL-7604244). D. Decrop is financially supported by the Agency for Innovation by Science and Technology in Flanders (IWT 121615).

Supporting Information

DMF-chip fabrication; construction of the Optical Tweezers set-up; magnetic bead characterization (zeta potentials and NIR absorbance); Experimental design and data analysis of the optimal design of experiments; extra tables and graphs of the statistical model.

Video illustrating the assembly of a smiley with magnetic beads using the optical tweezers (AVI).

References

1. Barbee, K. D.; Huang, X.; *Anal. Chem,*. **2008,** 80, 997–1003.
2. Burgin, E.; Salehi-Reyhani, A.; Barclay, M.; Brown, A.; Kaplinsky, J.; Novakova, M.; Neil, M. A. A.; Ces, O.; Willison, K. R.; Klug, D. R.; *Analyst*, **2014**, 139, 3235–44.
3. Cretich, M.; Damin, F.; Chiari, M.; *Analyst*, **2014**, 139, 528–42.

4. Romanov, V.; Davidoff, S. N.; Miles, A. R.; Grainger, D. W.; Gale, B. K.; Brooks, B. D.; *Analyst*, **2014**, 139**,** 1303–26.
5. Ma, H.; Horiuchi, K. Y.; *Drug Discov. Today*, **2006**, 11**,** 997–1003.
6. Kwon, C. H.; Wheeldon, I.; Kachouie, N. N.; Lee, S. H.; Bae, H.; Sant, S.; Fukuda, J.; Kang, J. W.; Khademhosseini, A.; *Anal. Chem.*, **2011**, 83, 4118–4125.
7. Xu, F.; Wu, J.-H.; Wang, S.; Durmus, N. G.; Gurkan, U. A.; Demirci, U.; *Biofabrication*, **2011**, 3, 034101.
8. Chen, J.; Li, J.; Sun, Y.; *Lab Chip*, **2012**, 12, 1753–67.
9. Yu, X.; Hartmann, M.; Wang, Q.; Poetz, O.; Schneiderhan-Marra, N.; Stoll, D.; Kazmaier, C.; Joos, T. O.*; PLoS One*, **2010**, 5, 1–7.
10. Lim, C. T.; Zhang, Y.; *Biosens. Bioelectron.*, **2007**, 22, 1197–204.
11. Sochol, R. D.; Casavant, B. P.; Dueck, M. E.; Lee, L. P.; Lin, L.; *J. Micromech. Microeng*, **2011**, 21, 1-8.
12. Kim, H.; Kim, J. ; *Microfluid. Nanofluidics*, **2014**, 16, 623–633.
13. Tan, W.-H.; Takeuchi, S.; *Lab Chip*, **2008**, 8, 259–66.
14. Attayek, P. J.; Hunsucker, S. A.; Wang, Y.; Sims, C. E.; Armistead, P. M.; Allbritton, N. L.*; Anal. Chem.*, **2015**, 87, 12281–89.
15. Verpoorte, E.; *Lab Chip*, **2003**, 3, 60N–68N.
16. Teshima, T.; Ishihara, H.; Iwai, K.; Adachi, A.; Takeuchi, S.; *Lab Chip*, **2010**, 10, 2443–8.
17. Burger, R.; Reith, P.; Kijanka, G.; Akujobi, V.; Abgrall, P.; Ducrée, J.*; Lab Chip*, **2012**, 12, 1289–95.
18. Ng, J. K.-K.; Liu, W.-T.; *Anal. Bioanal. Chem.*, **2006**, 386, 427–34.
19. Witters, D.; Knez, K.; Ceyssens, F.; Puers, R.; Lammertyn, J.; *Lab Chip*, **2013**, 13, 2047-54.
20. Rissin, D. M.; Kan, C. W.; Campbell, T. G.; Howes, S. C.; Fournier, D. R.; Song, L.; Piech, T.; Patel, P. P.; Chang, L.; Rivnak, A. J.; Ferrell, E. P.; Randall, J. D.; Provuncher, G. K.; Walt, D. R.; Duffy, D. C.; *Nat. Biotechnol.*, **2010**, 28, 595–9.
21. Kim, H.; Lee, S.; Kim, J.; *Microfluid. Nanofluidics*, **2012**, 13, 835–844.
22. Tanyeri, M.; Ranka, M.; Sittipolkul, N.; Schroeder, C. M.; *Lab Chip*, **2011**, 11, 1786–94.
23. Zhu, Z.; Frey, O.; Ottoz, D. S.; Rudolf, F.; Hierlemann, A.; *Lab Chip*, **2012**, 12, 906–15.
24. Iwai, K.; Takeuchi, S.; *Proc. IEEE Micro Electro Mech. Syst.*, **2009**, 371–374.
25. Iwai, K.; Tan, W.-H.; Ishihara, H.; Takeuchi, S.; *Biomed. Microdevices*, **2011**, 13, 1089–94.
26. Grier, D. G.; *Nature*, **2003**, 424, 810–6.
27. Eriksson, E.; Enger, J.; Nordlander, B.; Erjavec, N.; Ramser, K.; Goksör, M.; Hohmann, S.; Nyström, T.; Hanstorp, D.; *Lab Chip*, **2007**, **7,** 71–6.
28. Ozkan, M.; Wang, M.; Ozkan, C.; Flynn, R.; Birkbeck, A.; Esener, S.; *Biomed. Microdevices*, **2003**, 5, 61–67.
29. Wang, X.; Wang, Z.; Sun, D.; *Int. Conf. Control. Autom. Robot. Vis.*, **2010**, 7–10.
30. Wang, X.; Chen, S.; Kong, M.; Wang, Z.; Costa, K. D.; Li, R. A.; Sun, D.*; Lab Chip*, **2011**, 11, 3656–62.
31. Kovac, J. R.; Voldman, J.; *Anal. Chem.*, **2007**, 79, 9321–30.
32. Wang, X.; Gou, X.; Chen, S.; Yan, X.; Sun, D.; *J. Micromech. Microeng.*, **2013**, 23, 1-12.

33. Chen, B.; Lim, S.; Kannan, A.; Alford, S. C.; Sunden, F.; Herschlag, D.; Dimov, I. K.; Baer, T. M.; Cochran, J. R.*; Nat. Chem. Biol.*, **2015**, 12, 1–9.
34. Lane, R. E.; Korbie, D.; Anderson, W.; Vaidyanathan, R.; Trau, M.; *Sci. Rep.*, **2015**, 5, 7639.
35. Im, H.; Shao, H.; Park, Y.; Peterson, V. M.; Castro, C. M.; Weissleder, R.; Lee, H.*; Nat. Biotechnol.*, **2014**, 32, 490–5.
36. Poberaj, I.; Babic, D.; Osterman, N.; Kotar, J.; Vilfan, M.; Kavcic, B.*; Proc. SPIE*, **2008**, 7038.
37. Dimova, R.; Pouligny, B.; *Scatt. Shap. L. Beams App., G. Gouesbet*, Research Signpost, Trivandrum (**2000)**.
38. Zhou, Z.; Miller, H.; Wollman, A.; Leake, M.; *Photonics*, **2015**, 2, 758–772.
39. Ambardekar, A. A.; Li, Y.; *Opt. Lett.*, **2005**, 30, 1797–1799.
40. Vergauwe, N.; Witters, D.; Ceyssens, F.; Vermeir, S.; Verbruggen, B.; Puers, R.; Lammertyn, J..*; J. Micromech. Microeng.*, **2011**, 21, 1-11.
41. Lee, W. M.; Reece, P. J.; Marchington, R. F.; Metzger, N. K.; Dholakia, K.; *Nat. Protoc.*, **2007**, 2, 3226–38.
42. Goos, P.; Jones, B. *Optimal Design of Experiments - A Case Study Approach*. 1th ed.; Wiley: United Kingdom, 2011.
43. Agresti, A.; *Categorical Data Analysis*. 2nd ed.; Wiley Intersci.: New Jersey, 2002.
44. Neuman, K. K. C.; Nagy, A.; *Nat. Methods*, **2008**, 5, 491–505.
45. Lee, J.-G.; Cheong, K. H.; Huh, N.; Kim, S.; Choi, J.-W.; Ko, C.*; Lab Chip*, **2006**, 6, 886–895.
46. Urban, A. S.; Carretero-Palacios, S.; Lutich, A. A.; Lohmüller, T.; Feldmann, J.; Jäckel, F.*; Nanoscale;* **2014**, 6, 4458–74.
47. Agayan, R. R.; Horvath, T.; McNaughton, B. H.; Anker, J. N.; Kopelman, R.; *Proc. SPIE*, **2001**, **5514,** 502–513.
48. Palacios, S.; Romero-Rochin, V.; Volke-Sepulveda, K.; **2011**, at <http://arxiv.org/abs/1108.3316>
49. Dunderdale, G. J.; Howse, J. R.; Fairclough, J. P. A.; *Langmuir*, **2011**, 27, 11801–11805.
50. Shi, C.; Chan, D. Y. C.; Liu, Q.; Zeng, H.; *J. Phys. Chem. C*, **2014**, 118, 25000–25008.
51. Hoy, O.; Zdyrko, B.; Lupitskyy, R.; Sheparovyck, R.; Aulich, D.; Wang, J.; Bittrich, E.; Eichhorn, K.-J.; Uhlmann, P.; Hinrichs, K.; Müller, M.; Stamm, M.; Minko, S.; Luzinov, I.*; Adv. Funct. Mater.*, **2010**, 20, 2240–2247.
52. Lee, J. H.; Meredith, J. C.; *Langmuir*, **2011**, 27, 10000–10006.
53. Preuss, M.; Butt, H.-J.; *Langmuir*, **1998**, 14, 3164–3174.
54. Thormann, E.; Simonsen, A. C.; Hansen, P. L.; Mouritsen, O. G.; *Langmuir*, **2008**, 24, 7278–7284.
55. Faghihnejad, A.; Zeng, H.; *Langmuir*, **2013**, 29, 12443–12451.
56. Israelachvili, J.; Pashley, R.; *Lett. to Nat.*, **1982**, 300, 341–342.
57. Invitrogen|Dynal®. Surface-activated Dynabeads. *Invit. manuals* (**2010**).
58. Leckband, D.; Israelachvili, J.; *Q. Rev. Biophys.*, **2001**, 34.
59. Claesson, P. M.; Kjellin, M.; Rojas, O. J.; Stubenrauch, C.; *Phys. Chem. Chem. Phys.*, **2006**, 8, 5501–5514.
60. May, B.; Mahmood, E.; Al-koofee, D. A. F.; *Glob. J. Sci. Front. Res. Chem.*, **2013**, 13.
61. Treuel, L.; Eslahian, K. A.; Docter, D.; Lang, T.; Zellner, R.; Nienhaus, K.; Nienhaus, G. U.; Stauber, R.

H.; Maskos, M.*; Phys. Chem. Chem. Phys.*, **2014**, 16, 15053–67.

62. Nieminen, T. A.; Preez-Wilkinson, N. D.; Stilgoe, A. B.; Loke, V. L. Y.; Bui, A. A. M.; Rubinsztein-Dunlop, H.*; J. Quant. Spectrosc. Radiat. Transf.*, **2014**, 146, 59–80.

ToC figure